# Transmittance investigation on capacitive mesh on thick dielectric substrates as output windows for optically pumped terahertz lasers*

Qi Chun-Chao(祁春超), Zuo Du-Luo(左都罗), Lu Yan-Zhao(卢彦兆), Tang Jian(唐 建), and Cheng Zu-Hai(程祖海)†

*Wuhan National Laboratory for Optoelectronics, College of Optoelectronic Science and Engineering, Huazhong University of Science and Technology, Wuhan* 430074, *China*

(Received 5 October 2009; revised manuscript received 19 April 2010)

This paper reports that an output window for optically pumped terahertz (THz) laser has been fabricated by depositing a capacitive nickel-mesh on a thick high-resistivity silicon substrate (approximating to 5 mm thick). Unlike the conventional process of depositing a gold film approximating to 100 nm on negative photoresist using electron-beam evaporation, a nickel film approximating to 1.5 $\mu$m thick is directly deposited on the clean surface of dielectric substrate using magnetron sputtering and then a positive photoresist is spun onto the nickel metal surface at 6000 r for 60 s. A transmittance spectrum of the output window in a certain frequency range (say, from zero to 1 THz) has been obtained by using THz time domain spectroscopy. Moreover a transmittance spectrum simulated numerically has also been estimated with respect to the output window using the transmission-line model (TLM) containing attenuation component from dielectric substrate. The simulation results show that the TLM can explain well the experimental curve in a certain frequency range from zero to 1 THz. Thus it is demonstrated that the improved optical component can be efficiently used as both output coupler and output window for optically pumped THz lasers.

**Keywords:** physical optics, capacitive mesh structure, output coupler, optically pumped Terahertz laser

**PACC:** 4225, 0762, 4255D, 8115

## 1. Introduction

The output coupler is an extremely important optics component in optically pumped terahertz (THz) lasers[1−3] or far-infrared lasers.[4] Unlike the past hole couplers and freestanding mesh couplers,[5−9] in our experimental scheme, the output coupler also as sealed output window for the THz laser was fabricated by depositing metal nickel on high-resistivity silicon, and then using photolithography procedure[10,11] on the nickel films to obtain capacitive mesh configuration. The output window is required to reflect a part of THz radiation back into the laser cavity while allowing a certain percentage of THz radiation to be transmitted. The uses of the output windows instead of hole mirrors guarantee uniform output coupling over the entire zone of the waveguide, resulting in a low diverging Gaussian beam and relatively high output powers.[12,13] On the other hand, the integration design of the freestanding mesh coupler and the sealed window makes it more convenient to perform aligning adjustment of F–P cavity with the He–Ne laser beam. High resistivity silicon grown by the floating-zone method[14] has been shown to be extremely low loss below 3 THz[15] and thus is typically chosen as the substrate material of the output coupler. However, as the output coupler is used as output window, the substrate must be thickened sufficiently to enhance the mechanical strength required to support the extremely large pressure difference between the two surfaces of the substrate. Therefore the theoretical model (transmission-line model (TLM),[16] say) should consider the absorption component from the thick substrate. Moreover, the thickness of the metal film should be larger than the skin-depth at desired wavelength range in order to minimise losses.[17] However the conventional electron-beam evaporation can not deposit micrometer scale thick film, otherwise the metal thin film is easy to fall from the surface of the substrate due to the nonuniform stress. Here we use magnetron sputtering which may deposit metal nickel

*Project supported by the Creative Foundation of Wuhan National Laboratory for Optoelectronics (Grant No. Z080007) and partly by the National Basic Research Program of China (973 Program)(Grant No. 61328).

†Corresponding author. E-mail: chengzuhai@mail.hust.edu.cn

© 2010 Chinese Physical Society and IOP Publishing Ltd

on the surface of the high-resistivity silicon substrate at a rate of 1 $\mu$m per 2.5 min and the metal thin film is robust.

In this paper, unlike the conventional process of depositing a gold film (approximating to 100 nm) on a negative photoresist using electron-beam evaporation, here we utilise magnetron sputtering technique to deposit directly a considerably thick nickel film (approximating to 1.5 $\mu$m) on the clean surface of dielectric substrate, and then spin the positive photoresist onto the surface of nickel film at 6000 r for 60 s, finally a capacitive nickel-mesh structure was applied to the thick substrate by use of a photolithography process similar to that found in the Ref. [10]. The transmittance spectrum of the output window can be well explained by TLM containing the attenuation component of dielectric substrate.

## 2. Design and fabrication

Our output window for optically pumped THz laser consists of the capacitive nickel-mesh and high-resistivity silicon substrate ($\rho > 1$ k$\Omega$·cm) is shown in Fig. 1. The capacitive mesh material is made of metal nickel instead of gold, because the gold target is more expensive than the nickel target, whereas both of them have high reflectivities more than 99%.[11] The capacitive-mesh has been designed as the periodic square island with $g = 77$ $\mu$m, separated by a gap of width $2a = 28$ $\mu$m. The capacitive-mesh structure is somewhat easier to be fabricated and have the additional advantage of covering a larger portion of the surface with nickel, which helps to reflect the infrared (IR) radiation, thereby protecting IR-absorbing substrate from damage. The high-resistivity silicon substrate was polished into a plane-parallel etalon with 61 mm-diameter and approximate 5 mm-thickness. We change the conventional process procedure for our purposes in the progress of mesh fabrication. Our mesh fabrication procedure began with thorough cleaning of the substrate with acetone solvents and water, followed by a 105 °C dehydration bake for 20 min to remove any water. Then the substrate was placed above the nickel target in the magnetron sputter, and 1.5 $\mu$m thick nickel film was deposited onto the surface after 3.8 min. A positive photoresist was spun onto the nickel surface at 6000 r for 60 s and baked for 30 min at 95 °C. We imprinted a capacitive-mesh pattern in the photoresist by covering the substrate with a chromium-mesh photomask and a 17 s exposure to near ultraviolet. To complete the photolithography a RZX-3038 developer was utilised in the substrate for approximate 2 min and then the substrate was rinsed with water for 30 s. To protect the edges of each square island of capacitive-mesh the output window was baked for 30 min at 130 °C, after cooling for 10 min the exposed metal nickel was etched in mixed acid for 2 min and then was immediately rinsed in de-ionised water for 2 min to remove any residual acid. The last step was to remove photoresist covered on the square nickel islands with an ultrasonic acetone bath. After a series of processes the nickel mesh pattern as shown in Fig. 2 was formed.

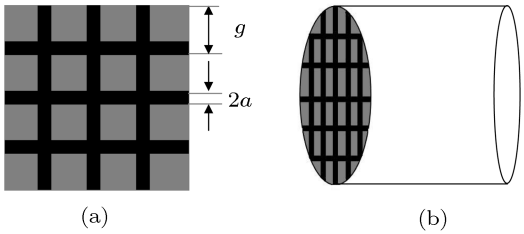



**Fig. 1.** (a) Schematic diagram of capacitive-mesh with gap width $2a$ and mesh period $g$ deposited on the surface of silicon substrate, (b) schematic diagram of the output window consisting of capacitive-mesh with 77 $\mu$m-wide square nickel mesh spaced every 28 $\mu$m.

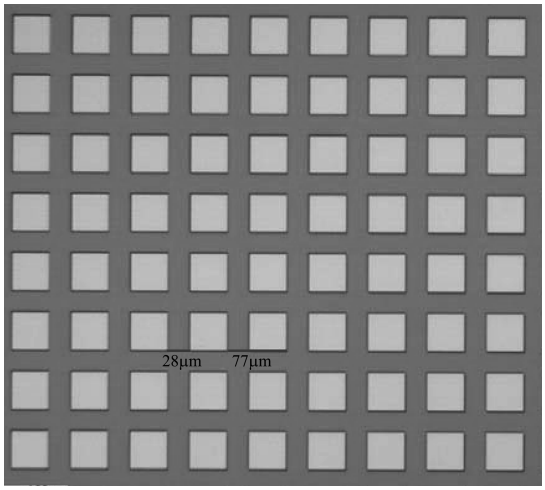



**Fig. 2.** Structure drawing of capacitive nickel-mesh with mesh period $g \approx 77$ $\mu$m and gap width $2a \approx 28$ $\mu$m.

## 3. Experiment and results

Figure 3 shows the general optical configurations of THz-TDS (time domain spectroscopy). The output window specimen was placed on the X–Y stage. Ultrashort laser pulses were guided to the expanding telescope formed by lens L1 and L2. The expanding telescope was selected to obtain approximately 4 mm

beam diameter size. Half-wave plate HWP1 and polariser P1 were used to split part of pumping power for pumping THz emitter. Emitter pumping beam then were directed to the optical delay line based on hollow retro-reflector HLR1, guided by the mirrors M3 and M4 to the THz emitter. Lens L3 focuses pumping beam to the gap of photoconductive antenna. Half-wave plate HWP2 and polariser P2 were used to adjust THz detector pumping power. Mirrors M5 and M6 were used to guide pumping beam to the THz detector. Lens L4 focuses pumping beam to the gap of photoconductive antenna. The THz radiation was focused to the output window specimen by lens L5. Lens L6 collimated the THz radiation to the THz detector. Iris diaphragms ID1–ID6 were used to facilitate beam guiding from laser to the THz emitter and detector. The signal from THz detector is detected by lock-in amplifier SR-810 (Stanford Research Systems).

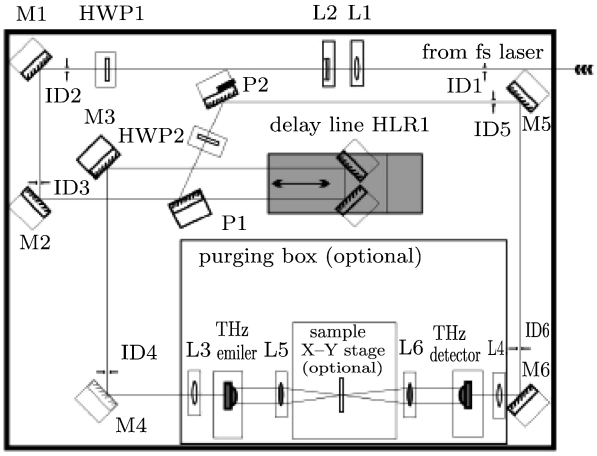



**Fig. 3.** General optical configurations of THz-TDS. Where L1–L6 are lenses; M1–M6 are mirrors; ID1–ID6 are iris diaphragms; HWP1 and HWP2 are half-wave plates; P1 and P2 are polarisers; HLR1 is hollow retro-reflector. The measured specimen is placed on the X–Y stage.

By scanning optical delay line, the waveforms of electrical fields of THz radiations entering the specimen (reference light) and passing through the specimen (transmitted light) were built as shown in Fig. 4. The transmittance spectrum of the window specimen was shown in Fig. 5.

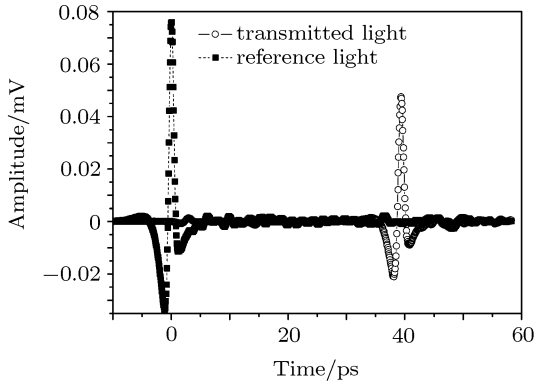



**Fig. 4.** Time-domain waveforms of reference light and transmitted light.

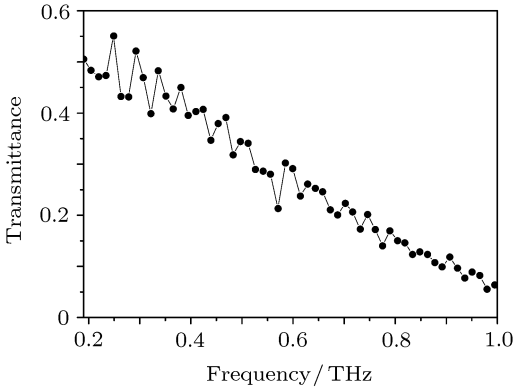



**Fig. 5.** Transmittance spectrum of the output window.

Figure 5 shows that there is a progressive decrease trend in the transmittance with the frequency increasing from zero to 1 THz. However, the transmittance spectrum has a slow oscillation in a narrow interval near a certain central frequency as a result of multiple internal reflections within the THz transparent substrate. For example, in a narrow interval of 0.365 THz to 0.394 THz near the central frequency 0.380 THz, the transmittance increases from 41% to the maximum value 45% then decreases to 39%, where the central frequency 0.380 THz corresponds to the maximum transmittance value of 45%.

## 4. Simulations and discussions

In this paper we applied the TLM [16] in the mesh coupler with loss dielectric substrate. The total intensity transmittance $T$ of the output window shown in Fig. 1(b) can be calculated directly in a manner analogous to that of Ohba and Ikawa[14] for a dielectric slab,

$$T = \frac{T_1 T_2 \exp(-\alpha t)}{1 + R_1 R_2 \exp(-2\alpha t) - 2\sqrt{R_1 R_2}\exp(-\alpha t)\cos(2\theta + 2\delta)}, \tag{1}$$

where $\alpha$ is the silicon substrate attenuation constant, and for high resistivity silicon ($\rho > 1$ k$\Omega$·cm) grown by the floating-zone method, there is a low absorption coefficient of $\alpha \leq 0.1$ cm$^{-1}$;[7] $\theta = -2\pi n_2 t/\lambda$ is the usual phase, where $t$ is the thickness of the substrate, $\lambda$ is the wavelength and $n_2$ is refractive index of dielectric substrate; $\delta$ is the phase shifts associated with reflection by any mesh at a dielectric boundary; $T_1$ and $R_1$ are the transmissivity and reflectivity in the first surface of the substrate, respectively; $T_2$ and $R_2$ are the transmissivity and reflectivity of the second surface, respectively. According to the TLM mentioned previously, these variables can be written as

$$T_2 = \frac{4n_1 n_2}{(n_1 + n_2)^2}, \tag{2}$$

$$R_2 = \frac{(n_1 - n_2)^2}{(n_1 + n_2)^2}, \tag{3}$$

$$T_1 = \frac{4n_1 n_2\left[\left(\dfrac{R_0}{Z_\mathrm{s}}\right)^2 + \left(\dfrac{X}{Z_\mathrm{s}}\right)^2\right]}{\left[1 + (n_1 + n_2)\dfrac{R_0}{Z_\mathrm{s}}\right]^2 + (n_1 + n_2)^2\left(\dfrac{X}{Z_\mathrm{s}}\right)^2}, \tag{4}$$

$$R_1 = \frac{\left[1 + (n_2 - n_1)\dfrac{R_0}{Z_\mathrm{s}}\right]^2 + (n_2 - n_1)^2\left(\dfrac{X}{Z_\mathrm{s}}\right)^2}{\left[1 + (n_1 + n_2)\dfrac{R_0}{Z_\mathrm{s}}\right]^2 + (n_1 + n_2)^2\left(\dfrac{X}{Z_\mathrm{s}}\right)^2}, \tag{5}$$

$$\delta = -\frac{1}{2}\arccos\left(\frac{-\left\{1 + (n_2^2 - n_1^2)\left[\left(\dfrac{R_0}{Z_\mathrm{s}}\right)^2 + \left(\dfrac{X}{Z_\mathrm{s}}\right)^2\right] + 2n_2\dfrac{R_0}{Z_\mathrm{s}}\right\}}{\sqrt{\{1 + (n_2^2 - n_1^2)\left[\left(\dfrac{R_0}{Z_\mathrm{s}}\right)^2 + \left(\dfrac{X}{Z_\mathrm{s}}\right)^2\right] + 2n_2\dfrac{R_0}{Z_\mathrm{s}}\}^2 + 4n_1^2\left(\dfrac{X}{Z_\mathrm{s}}\right)^2}}\right), \tag{6}$$

where $n_1$ is the refractive index of air, $Z_\mathrm{s}$ is the impedance of free space, $R_0$ is mesh loss resistance and $X$ is the reactance of the mesh. And these variables are given by

$$\frac{R_0}{Z_\mathrm{s}} = \sqrt{\frac{4\pi\varepsilon_0 c}{\lambda\sigma}}\frac{\eta}{4}, \tag{7}$$

$$\frac{X}{Z_\mathrm{s}} = \frac{2}{n_1^2 + n_2^2}\left(4\omega_0' \ln\left(\csc\left(\frac{\pi a}{g}\right)\right)\right)^{-1} \times \left(\frac{\omega}{\omega_0{}'} - \frac{\omega_0'}{\omega}\right), \tag{8}$$

$$\omega_0{}' = \omega_0\sqrt{\frac{2}{n_1^2 + n_2^2}}, \tag{9}$$

where $\varepsilon_0$ is the permittivity of free space, $c$ is the velocity of light, $\sigma$ is taken as one quarter of the bulk DC conductivity and $\eta = 1/(1-(2a/g))$ for capacitive mesh, $\omega_0'$ is the resonant frequency of the mesh at the dielectric interface and $\omega_0$ is the resonant frequency of the mesh in free space. In Fig. 6 we redraw the experimental curve and present simulation results of the transmittance spectra of the output window. To agree well with the experimental curve, one may change the resonant frequency $\omega_0$ and find that as $\omega_0 = 0.85$ theoretical and experimental curves have a good agreement. In the progress of numerical simulations, we have used some parameters: $n_1 = 1$, $n_2 = 3.418$, $t = 4.787$ mm, $\varepsilon_0 = 8.8542 \times 10^{-12}$ A·s·V$^{-1}$·m$^{-1}$, $c = 3 \times 10^8$ m·s$^{-1}$, $\sigma = 1.49 \times 10^{17}$ s$^{-1}$,[11] $\alpha = 0.01$ cm$^{-1}$, $2a = 28$ $\mu$m, $g = 77$ $\mu$m.

For the mesh output coupler with plane-parallel F–P substrate as described above, it is unavoidable to generate etalon effect, which has been an indisputable fact. However, in the process of simulation using TLM, the etalon effect was not found in the theoretical transmittance spectrum. We believe that the fast modulation can be found only if cosine component plays a dominant role in the denominator of Eq. (1), otherwise the theoretical transmittance spectrum is a smooth curve as shown in Fig. 6. Therefore, the TLM still need to be improved in the future.

Influences of the absorption coefficient and thickness of the substrate on the transmittance of the output window have been theoretically calculated in Fig. 7, respectively.

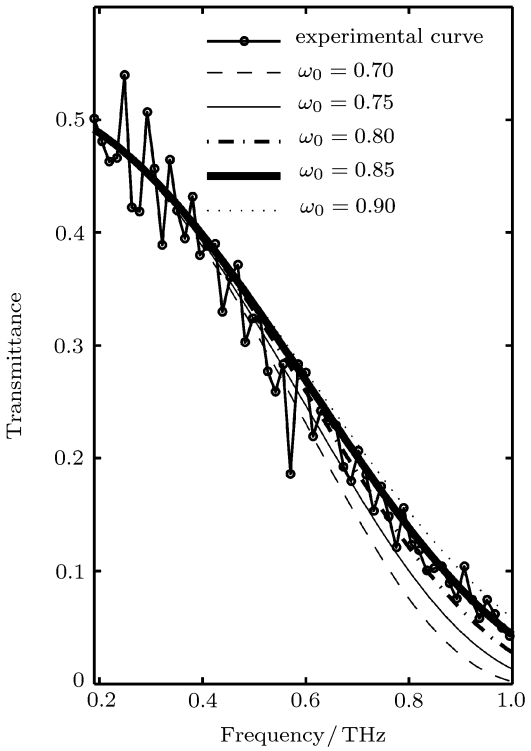



**Fig. 6.** Experimental curve and simulated transmittance spectra. Some parameters have been used here, for example $n_1 = 1$, $n_2 = 3.418$, $t = 4.787$ mm, $\varepsilon_0 = 8.8542 \times 10^{-12}$ A·s·V$^{-1}$·m$^{-1}$, $c = 3 \times 10^8$ m·s$^{-1}$, $\sigma = 1.49 \times 10^{17}$ s$^{-1}$, $\alpha = 0.01$ cm$^{-1}$, $2a = 28$ $\mu$m, $g = 77$ $\mu$m.

For the cases of the absorption coefficients less than 0.1 cm$^{-1}$, one may find that the transmittances vary slightly under a certain THz frequency, while shifting sharply as the absorption coefficient increases to 1 cm$^{-1}$. For example, near zero THz frequency there is a maximum transmittance difference less than 2% for the cases of the absorption coefficients less than 0.1 cm$^{-1}$, however a transmittance difference of about 16% is yielded for the case of $\alpha = 0.1$ cm$^{-1}$. Therefore, it is extremely necessary to select high-resistivity silicon to reduce THz absorption in silicon crystals. Actually, the thickness of the substrate is not a main problem to the THz transmittance. Figure 7 shows that the transmittance varies hardly as the thickness of the substrate varies from 2 to 5 mm, and that only a transmittance reduction less than 5% is yielded as the thickness increases by 15–18 mm. On the other hand, for a particular mesh period $g$ and the refractive index $n_2$ of the substrate, the onset of diffraction, for example the sharp dip at about 1.3 THz, can be determined at $\lambda = n_2 g$ near which the output window acts as a low-pass. As the mesh period $g$ increases, the onset of diffraction will shift toward the origin, resulting in a narrow bandpass. So for obtaining a wider bandpass, the mesh period $g$ must meet the relation of $g \leq \lambda/n_2$.

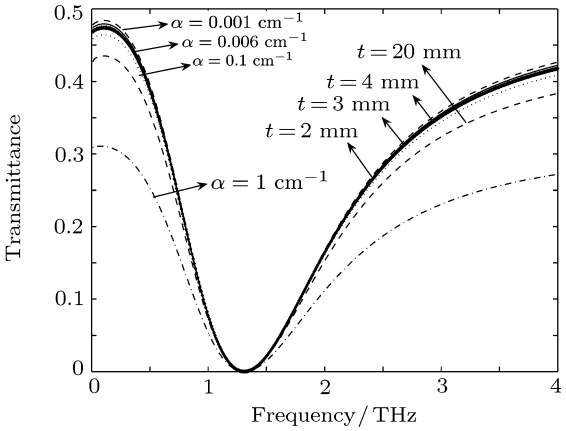



**Fig. 7.** Calculated transmittance spectra of the output window corresponding to various absorption coefficients for the same thickness of $t = 5$ mm and different substrate thicknesses for the same absorption coefficient of $\alpha = 0.06$ cm$^{-1}$.

## 5. Conclusion

In summary, we have fabricated an output window for optically pumped THz lasers by depositing a capacitive nickel-mesh on a high-resistivity silicon substrate approximating to 5 mm thickness. Unlike the conventional process of depositing a gold film approximating to 100 nm on negative photoresist using electron-beam evaporation, a nickel film approximating to 1.5 $\mu$m thickness has been directly deposited on the clean surface of dielectric substrate with the help of the magnetron sputtering and then a positive photoresist has been spun onto the nickel metal surface at 6000 r for 60 s. A progressive decrease trend in the transmittance for the output window in the frequency range from zero to 1 THz has been obtained by utilising THz-TDS. Moreover the transmittance spectra simulated numerically have also been estimated with respect to the output window using the TLM containing attenuation component from dielectric substrate. The simulation results show that as the resonant frequency $\omega_0 = 0.85$ is selected the TLM can agree well with the experimental curve in a certain frequency range from zero to 1 THz. Thus it is demonstrated that the improved optical component can be efficiently applied in the field of optically pumped THz lasers.

# References


[1] Qi C C, Zuo D L, Meng F Q, Lu Y Z, Jiu Z X and Cheng Z H 2009 *Acta Phys. Sin.* **58** 4641 (in Chinese)

[2] Qi C C and Cheng Z H 2009 *Chin. Phys. Lett.* **26** 064201-1

[3] Moretti A, Moruzzi G, Strumia F, Moraes J C S and Carelli G 2008 *IEEE J. Quantum Electron.* **44** 1104

[4] Bailey Jr W A, Gatesman A J, Gingras K R and Goodhue W D 2000 *Opt. Lett.* **25** 1349

[5] Wang J X, Qin Y L, Yan H Q, Gao P Q, Li J S, Yin M and He D Y 2009 *Chin. Phys.* B **18** 773

[6] Qin J Y, Zheng X S, Luo X Z, Huang X and Lin Y K 1998 *IEEE J. Quantum Electron.* **34** 32

[7] Liu H, Xu D G and Yao J Q 2008 *Acta Phys. Sin.* **57** 5662 (in Chinese)

[8] Telles E M, Moraes J C S, Scalabrin A, Pereira D, Moretti A and Strumia F 1991 *Appl. Phys.* B **52** 36

[9] Mueller E R, Wilson T E and Waldman J 1994 *Appl. Phys. Lett.* **64** 3383

[10] Scalari G, Ajili L, Faist J, Beere H, Davies G, Linfield E and Ritchie D 2003 *Appl. Phys. Lett.* **82** 3165

[11] Chen H and Wang L 2009 *Chin. Phys.* B **18** 2785

[12] MacDonald M, Alexnian A, York R A, Popovic Z and Grossman E N 2000 *IEEE Trans. Microwave Theory Tech.* **48** 712 6046

[13] Densing R, Erstling A, Gogolewski M, Gemund H P, Lundershausen G L and Gatesman A 1992 *Infrared Phys.* **33** 219

[14] Ohba T and Ikawa S I 1988 *J. Appl. Phys.* **64** 4141

[15] Grischkowsky D, Keiding S, van Exter M and Fattinger C 1990 *J. Opt. Soc. Am.* B **7** 2006

[16] Whitbourn L B and Compton R C 1985 *Appl. Opt.* **24** 217

[17] Winnewisser C, Lewen F and Helm H 1998 *Appl. Phys.* A **66** 593